PTCR Characteristics of Poly(styrene-*co*-acrylonitrile) Copolymer/Stainless Steel Powder Composites

Prativa Kar, Nilesh K. Shrivastava, Sumana Mallick, B. B. Khatua

Materials Science Centre, Indian Institute of Technology Kharagpur, Kharagpur-721 302, India

Received 7 March 2011; accepted 29 May 2011
DOI 10.1002/app.35002
Published online 5 October 2011 in Wiley Online Library (wileyonlinelibrary.com).

ABSTRACT: Positive temperature coefficient of resistivity (PTCR) characteristics of poly(styrene-co-acrylonitrile) copolymer (SAN)/stainless steel (SS) powder (80 wt %) composites prepared by melt-mixing method has been investigated with reference to SAN/carbon black (CB) composites. The SAN/CB (10 wt %) composites showed a sudden rise in resistivity (PTC trip) at 125°C, above the glass transition temperature (T_g) of SAN ($T_g \approx 107$°C). However, the PTC trip temperature of SAN/SS (80 wt %) composites appeared at 94°C, well below the T_g of SAN. Addition of 1 phr of nanoclay increased the PTC trip temperature of SAN/CB (10 wt %) composites to 130°C, while SAN/SS (80 wt %)/clay (1 phr) nanocomposites showed the PTC trip at 101°C. We proposed that the mismatch in coefficient of thermal expansion (CTE) between SAN and SS played a key role that led to a disruption in continuous network structure of SS even at a temperature below the T_g of SAN. The dielectric properties study of SAN/SS (80 wt %) composites indicated possible use of the PTC composites as dielectric material. DMA results showed higher storage modulus of SAN/SS composites than the SAN/CB composites. © 2011 Wiley Periodicals, Inc. J Appl Polym Sci 124: 607–615, 2012

Key words: carbon black; composites; resistivity; PTCR; glass transition

INTRODUCTION

The electrical conductivity of the insulating polymer can be achieved by the incorporation of conductive fillers into the polymer matrix above the percolation threshold, at which a continuous network of conductive particles is formed. Carbon black (CB), carbon fibers, graphite, metallic particles, intrinsically conductive polymers, and carbon nanotubes (CNTs) are widely used as fillers to get conducting polymer composites. An abrupt increase in resistivity (PTCR trip) near the melting temperature (T_m) of the semicrystalline or crystalline polymer matrix, converting the conducting composites to insulating one, is known as positive temperature coefficient to resistivity (PTCR) in conducting polymer composites. The PTCR composites can be used as auto controlled heater, current limiting devices and temperature sensor as the electrical resistivity of the composites increases sharply at a particular temperature. Many models have been proposed for explaining the mechanism, such as thermal expansion,[1,2] electron tunneling,[3–6] thermal fluctuation-included tunneling,[7] cooperative effect of changes in crystallinity and volume expansion,[8] and double percolation.[9–13]

Since last few decades, many researchers have investigated deferent aspect of PTCR phenomena for varieties of fillers filled composites. Most of the work has been done in order to eliminate negative temperature coefficient to resistivity (NTCR) effect that limits their application in over-temperature protections,[14–16] to increase PTC intensity,[17–19] reduce room temperature resistivity,[20] increase reproducibility and repeatability,[21,22] reduce the percolation threshold,[22–25] etc. Crosslinking of the semicrystalline polymer matrix by chemical and radiation methods has been reported to eliminate the NTCR effect.[14–16] The PTC intensity enhanced by surface treatment of CB with a grafting agent highly compatible with polymer matrix.[17,18] Jiang et al.[19] observed a sharp increase in resistivity near the T_m of the poly(vinylidene fluoride) (PVDF) in multiwall carbon nanotubes (MWCNTs)/PVDF nanocomposites. Zhou et al.[23] reported that the PTC trip of (80/20 and 20/80 w/w) linear low density polyethylene (LLDPE)/poly(ethylene methyl acrylate) (EMA) blends filled with CB appeared near the T_m of the major phase in the blends. Yang et al.[26] studied the PTC characteristics of high-density polyethylene (HDPE)/ethylene-vinylacetate (EVA)/CB composites and reported that the PTC trip of the composites correspond to the T_m of the major phase in which most of the filler were distributed. Liu and coworkers[27] reported the PTC trip temperature of bundle-like multiwalled carbon nanotube (MWCNTs) filled HDPE composites at 140°C, near the T_m of

Correspondence to: B. B. Khatua (khatuabb@matsc.iitkgp.ernet.in).

HDPE. Lee et al.[28] reported improvement in PTC intensity and repeatability in HDPE/CB composite in presence of small amount of MWCNT. Kalappa et al.[29] reported a significant volume expansion and noticeable PTCR effect in polyaniline (PANI)-MWCNT/CB/HDPE hybrid nanocomposites near the T_m of HDPE. Lisunova et al.[30] observed the PTCR effect above the T_m of the matrix polymer in ultrahigh molecular weight polyethylene (UHMWPE)/MWCNT composites. Gao et al.[31] reported that the PTC trip temperature of UHMWPE/CNT composites appeared around the T_m of the polymer, followed by a negative temperature coefficient of resistivity (NTCR). Li et al.[32] have reported a significant decrease in room temperature resistivity of HDPE/CB composites in presence of graphite nanofibers. However, the PTC trip temperature in both the composites appeared above the T_m of HDPE.

Most of the literature on PTCR polymer composites reports that PTCR trip temperature is a function of T_m or glass transition temperature (T_g) of the matrix polymer, and depends on polymer-filler combinations. Thus, the dimensional stability of the matrix polymer near the transition temperature (T_m or T_g) is a major concern that leads to the disadvantage of PTCR polymer composites. The objective of our work was to develop PTCR polymer composites with PTC trip temperature well below transition temperatures (T_m or T_g) of the matrix polymer. To explore this, we considered the coefficient of thermal expansion (CTE) values of polymer and conducting filler. If the matrix polymer had considerably high CTE value than the filler, the difference in CTE at high temperature could disrupt the continuous network of the filler-filler particles, making the composites insulating in nature. Thus, PTCR properties of styrene acrylonitrile (SAN)/stainless steel (SS) composites prepared by conventional melt processing method have been studied. The reason behind choosing SAN and SS was that SAN has high CTE value ($\approx$ 54 ppm/°C) than the SS ($\approx$ 16 ppm/°C). We found that the PTC trip temperature of SAN/SS composites appeared well below the T_g of SAN polymer. The electrical and thermal properties of the composites were investigated in detail and a plausible mechanism behind the PTCR effect has been proposed.

EXPERIMENTAL

Materials used

Poly(styrene-co-acrylonitrile) copolymer (SAN) used in this study was procured from ACROS Organics (25 wt % acrylonitrile and 75 wt % styrene random copolymer, $M_w \approx$ 165,000 g/mol). SS (316-L) was supplied by Alfa Aesar (A Johnson Mathey Company). Commercial grade conducting CB (Ketjenblack EC-300J, average particle size: 30 nm) was supplied by Akzo Nobel Chemicals, USA. The organoclay used in this study was Cloisite 20A (Southern Clay Product). It is a montmorillonite modified with dimethyl dihydrogenated tallow ammonium to increase the domain (d) spacing of Na^+-montmorillonite. The cation exchange capacity of Cloisite 20A is 95 mequiv/100 g of clay. Hereafter, Cloisite 20A is referred to as the clay.

TABLE I
Compounding Formulations for SAN/CB and SAN/SS Composites

SAN (g)	Carbon black (CB) (g)	Stainless steel (SS) (g)	Clay (phr) wrt. SAN
90	10	0	0
90	10	0	1
20	0	80	0
20	0	80	1
15	0	85	0

Preparation of the composites

Composites of SAN with CB and SS were prepared by conventional melt-blending method in an internal mixer (Brabender Plasticorder) at 200°C, with a rotor speed of 50 rpm for 20 min. Before the melt mixing, all the compounding ingredients were kept in air oven at 80°C for 24 h to avoid any moisture induced thermal degradation during mixing. All the ingredients in the composites formulation, as shown in Table I, were then dry mixed and fed into the internal mixer at 200°C for melt mixing. Finally, the composites were compression molded at 200°C into different shapes for further characterizations.

CHARACTERIZATION

Measurement of PTCR characteristics

Compression molded impact bar samples were fractured along the length at two ends under cryogenic condition. Hole with diameter of 1.5 mm and depth of $\approx$ 3 mm on centre of sample along the thickness was made on each sample, and a thermocouple was inserted to measure the actual sample temperature. Silver paint was applied on the fractured surfaces and dried at room temperature for 10 h. The sample was clamped with electrodes and with increasing temperature through uniform heating inside the oven, resistance was measured with a multimeter, and temperature was recorded across the sample with temperature indicator. The ambient temperature was controlled using the oven with an accuracy of $\pm$0.5°C. This process of measuring PTC characteristics is referred to as static measurement technique.

Alternative current (AC) and direct current (DC) voltage adjusted by a voltage controller was applied on the sample along the length direction, and the current passing through the sample was recorded using a digital multimeter. The heating behavior was characterized by measuring the surface temperature as a function of voltage and time. After the current and the surface temperature reached their steady values, the voltage was switched off and the sample was naturally cooled down to the room temperature. A higher voltage was then applied on the sample, and the same measurement procedure was performed. This process of measuring PTC characteristics is referred to as dynamic measurement technique.

Thermo mechanical analysis

Linear changes in sample dimension (CTE) as a function of temperature of the pure SAN and its composites were investigated through thermo mechanical analyzer (TMA, Perkin Elmer). The measurement was performed with the sample having length of 2.2 mm and cross-section area of 5.3 mm^2. The sample was scanned under nitrogen atmosphere from room temperature to 200°C at a heating rate of 5°C/min.

Differential scanning calorimetry study

The glass transition temperature (T_g) of pure SAN and that in the composites were determined with differential scanning calorimetry (DSC-200 PC, NETZSCH) with a heating rate of 10°C/min, under nitrogen atmosphere. The samples were heated from room temperature to 300°C, and then cooled to room temperature at a cooling rate of 10°C/min. The second heating scans were taken for determination of T_g of the sample.

Dielectric measurements

The dielectric and electrical properties of the SAN/SS (80 wt %) were obtained using a computer-controlled impedance analyzer (PSM 1735) on application of an alternating electric field across the sample cell with a blocking electrode (aluminum foil) in the frequency range of 50 Hz–10 MHz. The parameters like dielectric permittivity (ε') and dielectric loss tangent (tan δ) were obtained as a function of frequency. The AC conductivity (σ_{ac}) was calculated from the dielectric data using the relation:

$$\sigma_{ac} \approx \omega \varepsilon_0 \varepsilon' \tan \delta \quad (1)$$

where, ω is equal to $2\pi f$ (f is the frequency), and ε_0 is vacuum permittivity. The dielectric permittivity (ε') was determined with the following equation:

$$\varepsilon' \approx \frac{C_p}{C_0} \quad (2)$$

where C_p is the observed capacitance of the sample (in parallel mode) and C_0 is the capacitance of the cell. The value of C_0 was calculated using the area (A) and thickness (d) of the sample, following the relation:

$$C_0 \approx \frac{\varepsilon_0 A}{d} \quad (3)$$

DMA analysis

Dynamic modulus of the composites was measured by a dynamic mechanical analyzer (DMA 2980 model, TA Instruments Inc., USA). The dynamic temperature spectra of the composites were obtained in tension film mode at a constant vibration frequency of 1 Hz, temperature range of 30–150°C at a heating rate of 5°C/min, in nitrogen atmosphere. The dimension of the specimen was 30 × 6.40 × 0.45 mm^3.

Thermo gravimetric analysis

The thermal stability (onset degradation temperature: T_1) of the pure SAN and its composites was investigated with the help of thermo gravimetric analysis (TGA-209F, from NETZSCH). The sample was heated from room temperature to 600°C at a heating rate of 10°C/min, under air atmosphere.

RESULTS AND DISCUSSION

Temperature-resistivity study under static measurement

Figure 1 represents the variation of resistivity with temperature for the SAN/CB (10 wt %) and SAN/SS (80 wt %) composites at three consecutive heating cycles. As observed, room temperature resistivity of the SAN/CB (10 wt %) composites [Fig. 1(a)] did not show any remarkable changes up to 125°C. However, a sudden increase in resistivity of the composite was prominent at ≈ 130°C. For instance, room temperature resistivity (91.43 ohm cm) of the composites was increased to 23,334 ohm cm at 130°C. This indicated that SAN/CB (10 wt %) composite showed the PTCR trip temperature at ≈ 130°C, which was much higher than the glass transition temperature of SAN (T_g of SAN ≈ 107°C). It is a well known fact that, around the T_g polymer molecules absorb lot of heat, thus have lots of kinetic energy and the polymer chains can move around easily. Therefore after T_g, a reasonable volume expansion of polymer matrix takes place. We

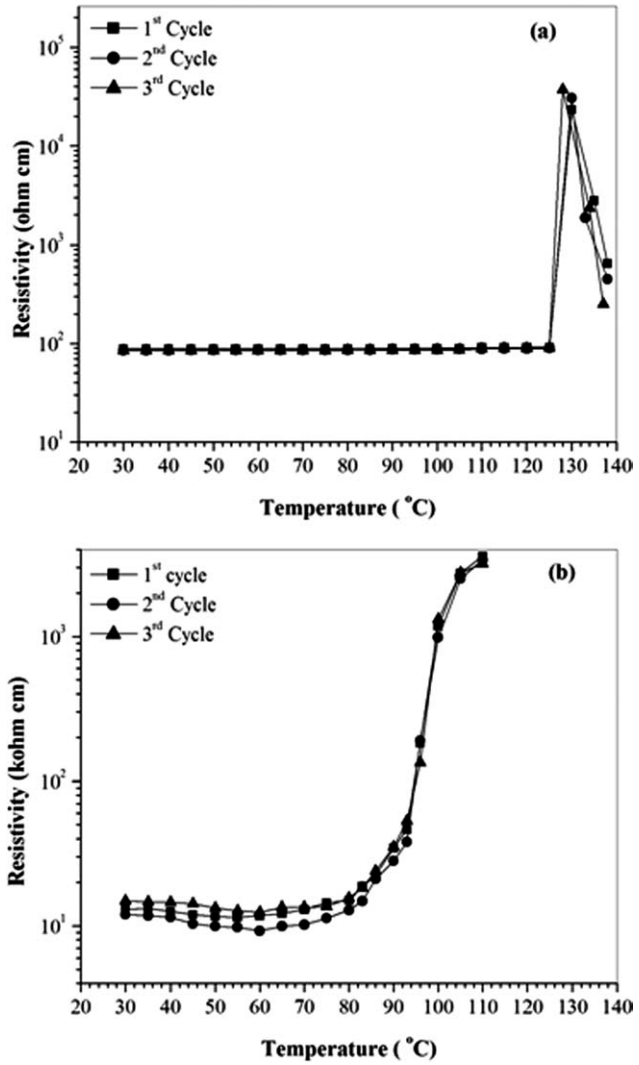

Figure 1 Resistivity-temperature curves of (a) SAN/CB (10 wt %) composites and (b) SAN/SS (80 wt %) composites at three consecutive heating cycles.

propose that, around 130°C the volume expansion of polymer matrix was enough to disrupt the continuous network structure of CB in the composites, leading to an increase in resistivity above the T_g of the matrix polymer (SAN). Not only the room temperature resistivity of SAN/CB (10 wt %) composites was stable but also the PTC trip of the composites did not change on thermal cycling.

Interestingly, the SAN/SS (80 wt %) composites showed the PTC transition at significantly low temperature region compared with that in SAN/CB (10 wt %) composites [Fig. 1(b)]. As observed, the room temperature resistivity (13 Kohm cm) of SAN/SS (80 wt %) composites significantly increased to 182.6 Kohm cm at a lower temperature of $\approx$ 94°C than that (130°C) of SAN/CB (10 wt %) composites. Thus, the PTCR trip temperature of SAN/SS (80 wt %) composites was well below the trip temperature of SAN/CB (10 wt %) composites, and the T_g (107°C) of SAN. Again, room temperature resistivity of SAN/SS (80 wt %) composites did not show any remarkable change with thermal cycling. As the trip temperature (94°C) of the composites was well below the T_g of SAN, SS particles could not move in the SAN matrix freely at the PTC trip temperature. Thus, formation of same continuous network of SS particles might be possible after cooling the composites to room temperature.

To explain the observed PTCR trip temperatures in SAN/SS (80 wt %) composites, we considered the CTE values of SAN and SS particles. It is well known that the CTE value of polymer (except heat shrinkable polymers) is higher than metallic and ceramic particles. The CTE of SAN ($\approx$54 ppm/°C) is remarkably higher than that of the SS (14–19 ppm/°C). Thus, in electrically conducting SAN/SS (80 wt %) composites, the SS particles formed a continuous network structure in SAN matrix. As the metal filler (SS) had lower CTE value, when compared with the matrix polymer (SAN), with increasing temperature the difference between the CTE values of the filler and polymer at certain temperature resulted in a disconnection (local phenomena) of filler-filler particles in the network structure. This disruption in filler-filler particle contact led to a sudden rise in electrical resistivity which results in the PTCR effect.

If the above assumption for the role of CTE mismatch on PTCR effect is true, then one can expect increase in PTC trip temperature of the SAN/SS composites having relatively lower CTE of the SAN matrix. To check this possibility, we studied the PTCR characteristics of SAN/SS (80 wt %)/clay composites. Addition of nanoclay is known to decrease the CTE of polymers in the nanocomposites.[33]

Figure 2(a) represents the TMA plots of pure SAN and SAN/clay (1 phr) and DSC heating scans of pure SAN, SAN/CB (10 wt %) composites, SAN/CB (10 wt %)/clay (1 phr), SAN/SS (80 wt %), SAN/SS (80 wt %)/clay (1 phr) and SAN/SS (85 wt %). It was observed [Fig. 2(a)] that there was a sharp increase in dimensions of SAN from 60°C, well below the T_g of the SAN. However, at certain temperature, the CTE value of pure SAN was considerably higher than that of SAN/clay (1 phr) nanocomposites. This indicates that, for similar volume expansion the nanocomposites will require relatively higher temperature (improvement in dimensional stability of polymer matrix) than that of the neat polymer (SAN). The high CTE value of polymers is generally caused by the low energy barrier for the chain conformation to be changed. The decrease in CTE value of SAN in the SAN/clay nanocomposites was due to the confinement of SAN chains inside the clay galleries. The high aspect ratio, stiff clay

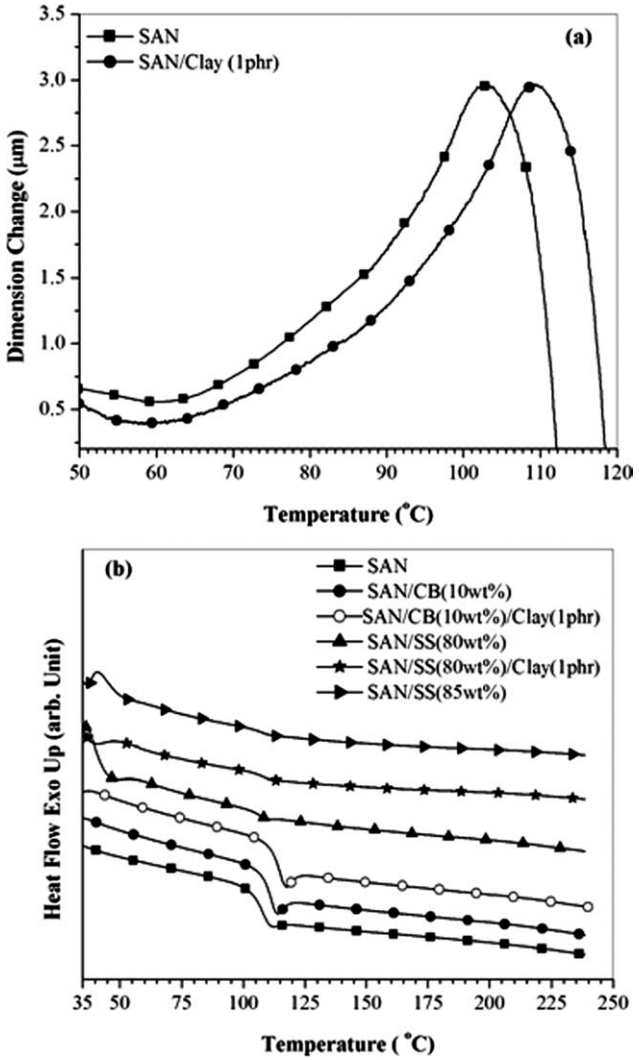

Figure 2 (a) TMA plots showing the change in volume with temperature for SAN and SAN/clay (1 phr) and (b) DSC thermograms of pure SAN, SAN/CB (10 wt %) composites, SAN/CB (10 wt %)/clay (1 phr) composites, SAN/SS (80 wt %) composites, SAN/SS (80 wt %)/clay (1 phr) composites, SAN/SS (85 wt %) composites.

platelets may act as barriers for the thermal diffusion process. Thus, the volumetric or linear thermal expansion coefficient of SAN was reduced in the nanocomposites. We assume that the extent of thermal expansion of SAN at 94°C was enough to disrupt the continuous network structure of SS particles, leading to sharp increase in the resistivity (PTC trip) value of the composites.

Figure 2(b) represents the DSC heating scans of pure SAN, SAN/CB (10 wt %) composites, SAN/SS (80 wt %) composites without and with 1 phr clay and SAN/SS (85 wt %) composites. The T_g of pure SAN was appeared at a temperature $\approx$ 107°C and remain unaffected in SAN/SS (80 wt %) and SAN/SS (85 wt %) composites. In SAN/CB (10 wt %) composites, the T_g was shifted to slightly higher temperature region (109°C) compared with that of pure SAN and further increased to 112°C in case of SAN/CB (10 wt %)/clay (1 phr) composites. The T_g of SAN/SS (80 wt %) was also increased to 110°C in presences of 1 phr clay. This increase in T_g of SAN in the nanocomposites was due to the confinement (intercalation) of SAN chain inside the clay galleries that restricted the segmental motion of matrix polymer SAN. Thus increase in T_g clearly indicated the intercalation of SAN inside the clay silicate layers in SAN/CB (10 wt %)/clay (1 phr) and SAN/SS (80 wt %)/clay (1 phr) composites.

Figure 3 shows the effect of nanoclay on the PTCR characteristics of SAN/CB (10 wt %) and SAN/SS (80 wt %) composites. The SAN/CB (10 wt %) composites with 1 phr of clay showed relatively lower room temperature resistivity ($\approx$ 80.7 ohm cm) compared with that without any clay ($\approx$ 88 ohm cm). This might be due to better dispersion of CB particles in SAN matrix in presence of clay. The CB clusters broke down during melt blending due to increased melt viscosity of SAN in presence of the clay which prevented the agglomeration of CB particles leading to better dispersion. Interestingly, the PTC trip temperature (130°C) of SAN/CB composites shifted to $\sim$ 136°C when the composite was formulated with 1 phr of the clay. The SAN/SS (80 wt %)/clay (1 phr) composites showed the PTCR transition at $\sim$ 101°C, which was also higher than that (94°C) of the composites without any clay. However, the PTC trip temperatures of SAN/SS (80 wt %) composites without and with 1 phr clay were lower than the T_g values of SAN in the respective composites. It is noteworthy that, the PTC trip temperatures of the SAN/SS (80 wt %) composites without and with clay (1 phr) were very similar to the temperatures that correspond to the similar CTE value

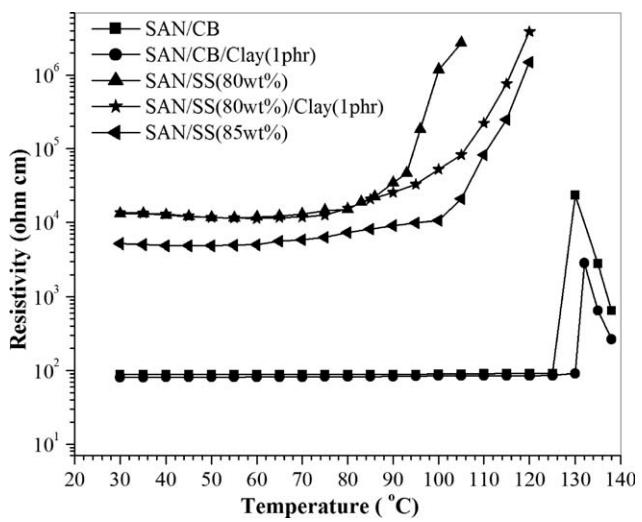

Figure 3 Resistivity-Temperature curves of SAN/CB (10 wt %) and SAN/SS (80 wt %) composites without and with clay.

of SAN and its nanocomposites with 1 phr of clay [Fig. 2(a)]. For instance, the change in dimension of pure SAN at ≈ 95°C was comparable with that of SAN/clay (1 phr) nanocomposites at ≈ 100°C. Thus, on the basis of PTCR characteristics and thermal behavior (DSC and TMA), we conclude that the mismatch in CTE values of SAN and SS at 94°C and 101°C were enough to break the continuous network structure of SS in SAN/SS (80 wt %) composites without and with 1 phr of clay, respectively.

If the CTE mismatch phenomena played a major role behind the PTCR effect in SAN/SS composites, one would expect an increase in the PTC trip temperature of the composites with increase in filler concentration. To check the possibility, we also investigated the PTCR characteristic of the composites with relatively higher loading level (85 wt %) of SS powder. As observed (Fig. 3), room temperature resistivity of SAN/SS (85 wt %) composites was lower (5.2 Kohm cm) than that (13 Kohm cm) of the composites with 80 wt % SS loading. This was due to the formation of more contact points in the continuous network structure of SS at higher loading that reduced the contact resistance in the composites. The PTC trip temperature of the SAN/SS (85 wt %) composites was shifted to ≈ 104°C, which was higher than that (94°C) of the composites with 80 wt % of SS loading. This result clearly indicated that at 85 wt % filler (SS) loading, the composites required higher volume expansion and hence higher temperature (PTC trip ≈ 105°C) to disrupt the filler-filler contact points in the continuous network structure, compared with that (94°C) in case of the composites with 80 wt % of filler loading.

To explain the difference in the PTCR trip temperature of SAN/CB (10 wt %) composites and SAN/SS (80 wt %) composites, we considered the particle size of the CB and SS powder. The average particle size (D) of CB used in this study was ≈ 30 nm, which was significantly smaller than the D of SS (≈ 40 μm). Thus, even at 10 wt % of CB loading, the number of CB particles and hence, CB-CB contact points and branching on the CB-CB particles continuous network structure in SAN/CB (10 wt %) composites were expected to be considerably higher than the branching of SS in SAN/SS (80 wt %) composites. Thus, the SAN/CB (10 wt %) composites required higher volume expansion and hence higher temperature to disrupt the CB-CB contact points in the continuous network structure than that of the SAN/SS (80 wt %) composites.

Studies on current (I)-voltage (V) characteristics and PTCR effect under dynamic measurement

Figure 4 presents the current-voltage dependence for SAN/SS composites at 80 wt % SS loading. It is clear from the figure that SAN/SS (80 wt %) composites show ohmic conduction. At room temperature, under both AC [Fig. 4(a)] and DC [Fig. 4(b)] applied voltage, the initial current (I) flow in the composites was increased with increasing the applied voltage. The maximum temperature rise in the composites at different AC and DC voltage applications was also investigated. When the applied voltage (AC or DC) was increased to ≈ 130 V, a maximum temperature of ≈ 97°C could be developed in the composites. Near the PTC trip temperature, current flow in the composites decreased as the resistance increased. Thus, there was no further increase in temperature of the composites above applied voltage (130 V), and the maximum temperature developed as a result of current flow was limited to the PTC trip temperature (≈ 94°C) of the composites.

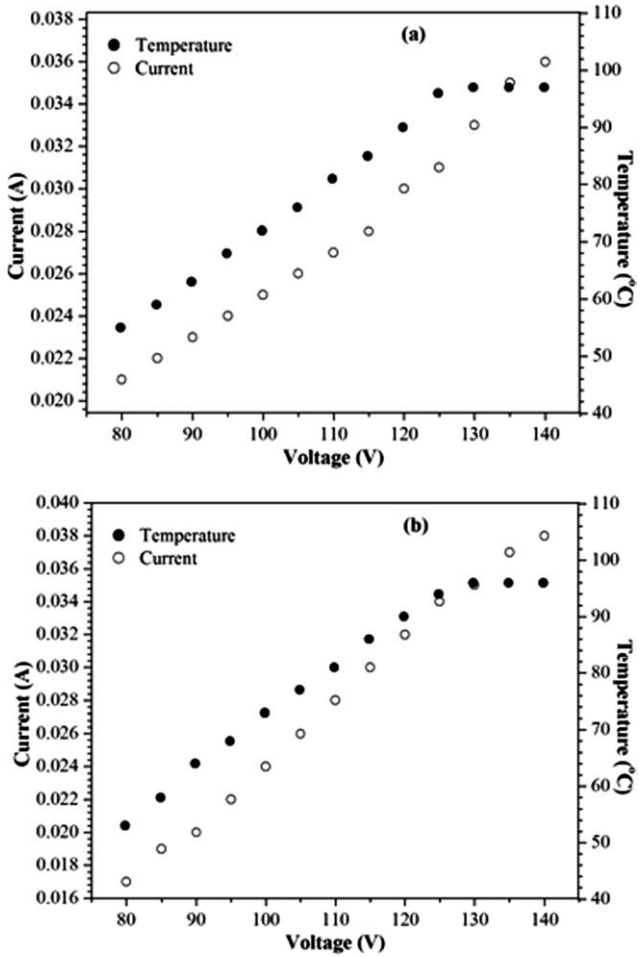

Figure 4 Current (I)-voltage (V) characteristics of SAN/SS (80 wt %) composites under (a) AC voltage and (b) DC voltage applications.

The thermo-electric behavior of SAN/SS (80 wt %) composites with time under 80 and 130 V applications are shown in Figures 5 and 6, respectively. It is interesting to note that, the temperature of the composites was increased to a maximum of 55°C and 53°C under 80 V AC and DC applications (Fig. 5),

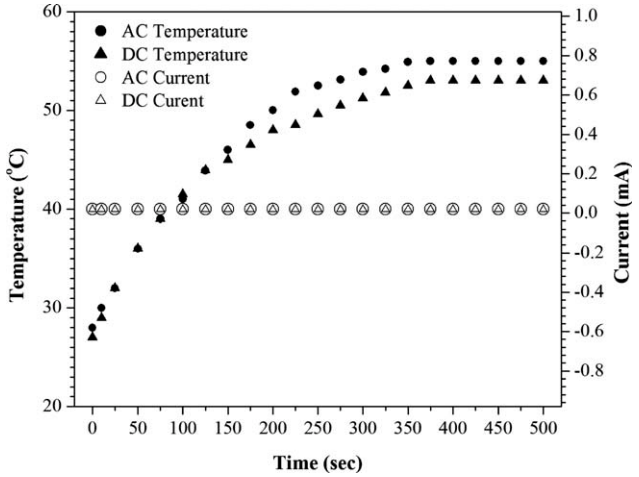

Figure 5 Temperature-current (*I*) plots of SAN/SS (80 wt %) composites under 80 V AC and DC applications.

respectively. At 80 V application (AC and DC), *I* of the composites remain constant with time. This observation was also supported by the temperature-resistivity measurement (Fig. 1) that indicated the room temperature resistivity of the composites remain almost constant at ≈ 55°C. However, under both AC and DC applications, a sharp decrease in *I* was evident after 125 s when the applied voltage was increased to 130 V (Fig. 6). As observed, under 130 V AC and DC application, the composites could attain ≈ 94°C after 125 s and 150 s, respectively, which were close to the PTC trip temperature of the SAN/SS (80 wt %) composites. Thus, increase in resistivity of the composites near the PTC trip temperature resulted in a decrease in *I* of the composites, and hence no further increase in temperature was observed.[34]

Dielectric properties

Figure 7 shows the variation of dielectric permittivity (ε′) of the SAN/SS (80 wt %) composites with frequency in a wide range (50Hz–10 MHz) at room temperature. A rapid decrease in dielectric permittivity of the composites was prominent at lower frequency region (up to 1 kHz) indicating dispersion at low frequency in dielectric constant, and then, a slow but gradual decrease in dielectric permittivity was observed with further increasing the frequency up to 1 MHz. The decrease of dielectric permittivity (ε′) with increasing frequency is the expected behavior in most dielectric materials. This might be due to the dielectric relaxation that involved the orientation polarization, which depend on the molecular arrangement and uniform dispersion of the filler aggregates throughout the sample. The dielectric permittivity of a material decreases with decrease in polarizability. At higher frequencies, the polar molecules of dielectric get less time to orient themselves in the direction of the alternating field; hence, dielectric permittivity decreases with increasing frequency.[35] A higher value of dielectric permittivity (ε′) at low frequency is due to the presence of all types of polarizations (i.e., electronic, ionic, dipolar, interfacial, etc.) in the sample at room temperature. As only the electronics polarization dominates at higher frequency (other types of polarizations vanish), the value of dielectric permittivity (ε′) decreases with increase in frequency. The variation of loss tangent also follows the identical pattern like that of dielectric permittivity (ε′). Figure 7 also shows the variation of dielectric loss tangent (tan δ) of the composites with frequency range (50 Hz–10 MHz) at room temperature. As observed, dielectric loss tangent was decreased with increase in frequency and became constant at 10^5 Hz. The decrease in dielectric loss tangent at higher frequency might be attributed to the dipole relaxation phenomena associated with

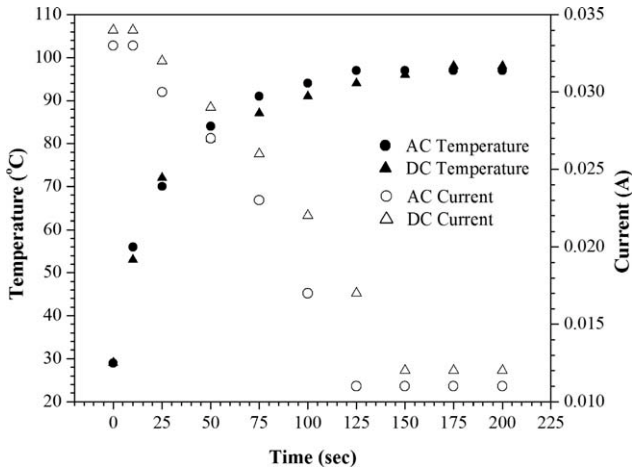

Figure 6 Temperature-current (*I*) plots of SAN/SS (80 wt %) composites under 130 V AC and DC applications.

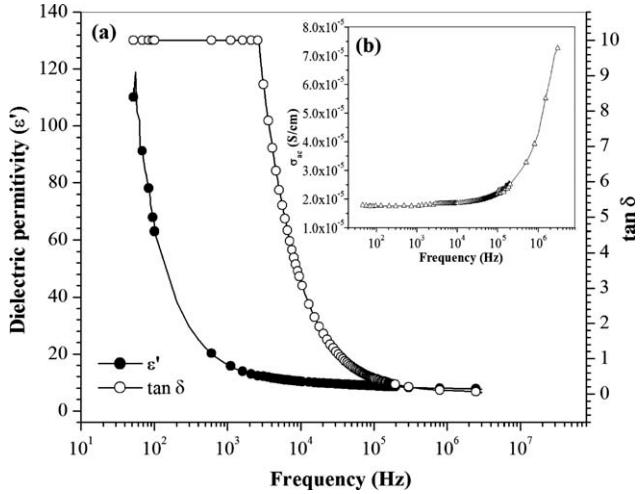

Figure 7 Variation of (a) dielectric permittivity (ε′) and dielectric loss (tan δ) with frequency and (b) ac conductivity (σ_{ac}) with frequency of SAN/SS (80 wt %) at room temperature.

the inability of the electric dipoles to be in the same phase with the frequency of applied electric field.

Figure 7 (inset) shows the variation of electrical conductivity of the SAN/SS (80 wt %) composites as a function of frequency (50 Hz–10 MHz) at room temperature. As can be seen, a marginal increase in conductivity of the composites was evident with increase in frequency up to 10^5 Hz. The increase in electrical conductivity with frequency was more prominent in the frequency range of 10^5 Hz–10^6 Hz. It is widely believed that their electrical properties of polymer composites depend primarily on the way the filler particles are distributed through the polymer matrix. The electrical conductivity, in the SAN/SS (80 wt %) composites was due to the formation of continuous network structure by the electrically conductive SS particles. The frequency dependence of conductivity in polymer composites is due to hopping transport between localized sites. The dispersion of SS filler is heterogeneous, localized, and disordered. The disorder dispersion of filler particles in polymer matrix results in a wide distribution of hopping rates giving a strong dispersion of the AC conductivity. The conduction mechanism has not yet been cleared due to complex polymer structure.[36]

In most polymer composites, a power law dependence of conductivity (σ) on variation in frequency (ω) is observed, which is represented mathematically by:

$$\sigma'(\omega) \alpha \omega^{\upsilon} \tag{4}$$

with the value of the exponential parameter, υ ranging from $0 < \upsilon \leq 1$, but mostly $\upsilon \approx 1$. The frequency dependence usually relates a small DC conductivity to a high localized one (at increasing frequencies) and is attributed to the polarization of the increasingly small conducting units. In disordered materials electron transport, the relevant mechanisms are electron localization with associated hopping[36] and fractal topology.[37] The electrical conductivity, σ, of many disordered solids including polymer composites was shown by Jonsacher[38] to consist of a frequency independent and a strongly frequency dependent component, the former being the DC conductivity, σ. From the experimental data in limited frequency region, it was noted that the overall frequency dependence of σ or the so called "universal dynamic response" of electron conductivity could be approximated by the following simple relation:

$$\sigma(\omega) = \sigma \mathrm{DC} + A\omega^{s} \tag{5}$$

where $\omega = 2\pi f$ is the angular frequency, and A and s are exponential parameters. For a polymer composite containing moderate concentration of filler, $s \approx 0.5$–0.6, and both s and A follow strong dependencies on a variety of factors including the filler loading and temperature.

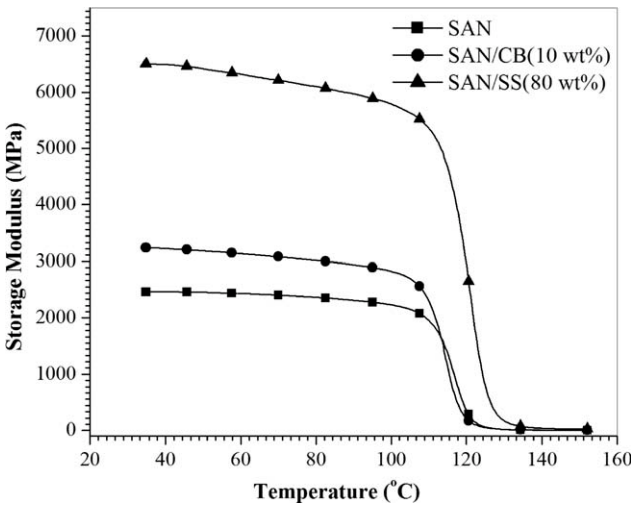

Figure 8 Storage modulus of pure SAN, and SAN/CB (10 wt %) composites, SAN/SS (80 wt %) composites.

Mechanical properties

Figure 8 represents the DMA plots of pure SAN and its composites with CB (10 wt %) and SS powder (80 wt %). As observed, the storage modulus of SAN was increased in both SAN/CB (10 wt %) and SAN/SS (80 wt %) composites throughout the entire temperature (30–160°C) scan. This might be due to the stress transfer from matrix to the filler. The storage modulus of SAN was significantly increased in SAN/SS (80 wt %) composites. This may be due to the presence of higher amount of filler in the polymer. Thus, the stress transfer from matrix to filler took place in a better manner, or we can say that the stress may be withstood by the high concentration filler. It is noteworthy, the storage modulus of the SAN/SS (80 wt %) composites at its PTCR trip temperatures is $\approx$ 100 times higher than that of SAN/CB (10 wt %) composites. This observation clearly indicated that SAN/SS (80 wt %) had remarkably high dimensional stability than the SAN/CB (10 wt %) composites at their PTCR trip temperatures.

Thermo gravimetric analysis

Figure 9 represents the TGA plots for pure SAN, SAN/CB (10 wt %) composites and SAN/SS (80 and 85 wt %) composites, without and with 1 phr clay. As observed, all the composites showed higher initial degradation temperature (T_1) compared with the pure SAN. The T_1 of SAN was significantly increased in SAN/SS (80 wt %) composites ($T_1 \approx 359$°C) compared to that ($T_1 \approx 335$°C) in the SAN/CB (10 wt %) composites. This increase in thermal stability may arise from the interaction between the polymer chains and the fillers surfaces.

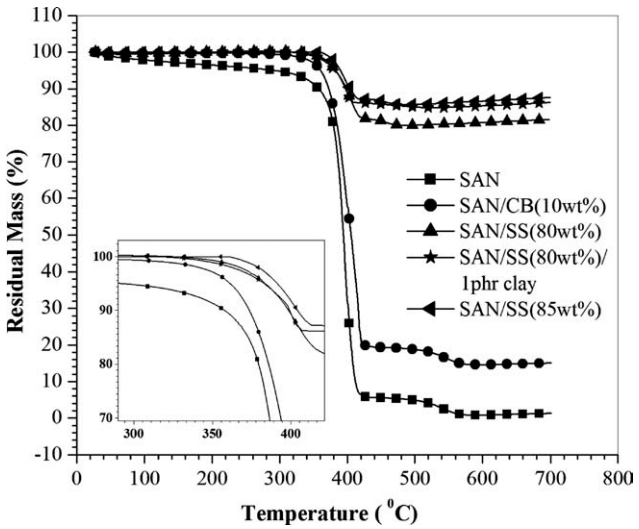

Figure 9 TGA thermograms of pure SAN, and its composites with CB (10 wt %), SS (80 wt %) without and with 1 phr clay and SAN/SS (85 wt %) composites.

The PTC trip temperature (≈ 94°C) of SAN/SS (80 wt %) composites was reasonably lower than the initial degradation temperature (359°C) of the composites. The high thermal stability of SAN/SS (80 wt %) composites indicates that the composites can be efficiently used as PTCR material without any thermal degradation on several cycling.

CONCLUSION

The effect of CTE of the matrix polymer and fillers on the PTCR behavior of SAN/SS composites was studied. The PTC trip temperature of SAN/SS (80 wt %) composites was observed well below the T_g of the matrix polymer (SAN). The composite exhibited almost the same room temperature resistivity and similar PTCR characteristics upon three consecutive thermal cycles. Addition of small amount of nanoclay in the composites, that reduced the CTE of SAN, shifted the PTCR trip temperature to higher temperature region in the composites. The PTCR trip of SAN/CB (10 wt %) composites appeared much above the T_g of the matrix polymer (SAN). This was due to higher volume expansion of SAN after the T_g, as evident from the TMA analysis. We proposed that the mechanism behind the PTCR effect in SAN/SS composites was a result of CTE mismatch between SAN and SS that could break-off and separate the particle-particle micro-contacts of filler in matrix polymer SAN. The CTE mismatch disrupted the continuous network structure of the conducting fillers even below the T_g of SAN. The prepared polymeric PTCR composites (SAN/SS) can be used as PTC materials for several cycles due to its significantly high thermal and dimensional stability with PTC trip temperature below the T_g of the matrix polymer.

References

1. Kohler, F. U.S. Pat. 3,243,753 (1966).
2. Park, S.-J.; Kim, H.-C.; Kim, H.-Y. J Colloid Interf Sci 2002, 255, 145.
3. Ohe, K.; Naito, Y. Jpn J Appl Phys 1971, 10, 99.
4. Meyer, J. Polym Eng Sci 1973, 13, 462.
5. Meyer, J. Polym Eng Sci 1974, 14, 706.
6. Costa, L. C.; Chakki, A.; Achour, M. E.; Graca, M. P. F. Phys B 2011, 406, 245.
7. Sherman, R. D.; Middleman, L. M.; Jacobsa, S. M. Polym Eng Sci 1983, 23, 36.
8. Luo, Y. L.; Wang, G. C.; Zhang, B. Y.; Zhang, Z. P. Eur Polym J 1998, 34, 1221.
9. Sumita, M.; Sakata, K.; Asai, S.; Miyasaka, K.; Nakagawa, H. Polym Bull 1991, 25, 265.
10. Gubbels, F.; Erome, R. J.; Teyssic, P. H. Macromolecules 1994, 27, 1972.
11. Feng, J.; Chan, C.-M. Polymer 2000, 41, 7279.
12. Zhang, X.; Pan, Y.; Polym Int 2008, 57, 770.
13. Zhang, M. Q.; Yu, G.; Zeng, H. M.; Zhang, H. B.; Hou, Y. H. Macromolecules 1998, 31, 6724.
14. Jia, W. T.; Chen, X. F.; Li, S. H. J Appl Polym Sci 1996, 60, 2317.
15. Narkis, M.; Vacam, A. J Appl Polym Sci 1984, 29, 1639.
16. Yang, H. Radiat Phys Chem 1993, 42, 135.
17. Adib, F.; Ko, C. C.; Liu, G. J.; Zhang, Z. R. U.S. Pat. 20,030,096,888 (2003).
18. Chu, E. F. H.; Wang, D. S. C.; Ma, Y. C. U.S. Pat. 20,030,111,648 (2003).
19. Jiang, S. L.; Yu, Y.; Xie, J. J.; Wang, L. P.; Zeng, Y. K.; Fu, M.; Li, T. J Appl Polym Sci 2010, 116, 838.
20. Yu, G.; Zhang, M. Q.; Zeng, H. M. J Appl Polym Sci 1998, 70, 559.
21. Zhang, J. F.; Zheng, Q.; Yang, Y. Q.; Yi, X. S. J Appl Polym Sci 2002, 83, 3112.
22. Su, C.; Wang, G.; Huang, F.; Sun, Y. J Macromol Sci Part B: Phys 2008, 47, 65.
23. Zhou, P.; Yu, W.; Zhou, C.; Liu, F.; Hou, L.; Wang, J. J Appl Polym Sci 2007, 103, 487.
24. Rybak, A.; Boiteux, G.; Melis, F.; Seytre, G. Comp Sci Technol 2010, 70, 410.
25. Boiteux, G.; Mamunya, Y. P.; Lebedev, E. V.; Adamczewski, A.; Boullanger, C.; Cassagnau, P.; Seytre, G. Synthetic Met 2007, 157, 1071.
26. Yang, Q.-Q.; Liang, J.-Z. J Appl Polym Sci 2010, 117, 1998.
27. Liu, F.; Zhang, X.; Li, W.; Cheng, J.; Tao, X.; Li, Y.; Sheng, L. Compos Part A 2009, 40, 1717.
28. Lee, J.-H.; Kim, S. K.; Kim, N. H. Scripta Materialia 2006, 55, 1119.
29. Kalappa, P.; Lee, J.-H.; Rashmi, B. J.; Venkatesha, T. V.; Pai, K. V.; Xing, W. IEEE Trans Nanotech 2008, 7, 223.
30. Lisunova, M. O.; Mamunya, Y. P.; Lebovka, N. I.; Melezhyk, A. V. Eur Polym J 2007, 43, 949.
31. Gao, J. F.; Li, Z. M.; Peng, S.; Yan, D. X. Polym Plast Tech Eng 2009, 48, 478.
32. Li, Q.; Siddaramaiah, B; Kim, N. H.; Yoo, G.-H.; Lee, J. H. Compos Part B: Eng 2009, 40, 218.
33. Chen, B.; Liu, S.; Evans, J. R. G. J Appl Polym Sci 2008, 109, 1480.
34. Kar, P.; Khatua, B. B. J Appl Polym Sci 2010, 118, 950.
35. Smyth, C. P. Dielectric Behavior and Structure, Vol. 53; McGraw Hill: New York, 1955.
36. Mahapatra, S. P.; Sridhar, V.; Chaudhary, R. N. P.; Tripathy, D. K. Polym Eng Sci 2007, 47, 984.
37. Bottger, H.; Bryskin, V. V. Hopping Conduction in Solids; Akademie-Verlag: Berlin, 1985.
38. Jonsacher, A. K. Nature 1979, 267, 673.